Journal of Materials Science: Materials in Electronics (2019) 30:11181–11192
https://doi.org/10.1007/s10854-019-01464-0

Effect of Nb^{3+} ion substitution on the magnetic properties of $SrFe_{12}O_{19}$ hexaferrites

M. A. Almessiere[1,2] · Y. Slimani[1,3] · S. Güner[4] · J. van Leusen[4] · A. Baykal[1] · P. Kögerler[1]

Received: 11 February 2019 / Accepted: 3 May 2019 / Published online: 8 May 2019

Abstract

The crystal structure and magnetic properties of $SrNb_xFe_{12-x}O_{19}$ ($0.00 \le x \le 0.08$) nanohexaferrites (NHFs) fabricated using a sol–gel technique is presented in this study. The X-ray powder diffractometry (XRD) and Infrared spectroscopy (FT-IR) confirmed the formation of M-type hexaferrite phase. The analyses of magnetization versus applied magnetic field, M(H), were performed at room (300 K; RT) and low (10 K) temperatures. The Bohr magneton number (n_B), saturation (M_s) and remanent (M_r) magnetization values increase slightly with increasing Nb^{3+} content. The room-temperature values of the magnetic parameters $M_r = 31.41$–33.28 emu/g, $M_s = 57.10$–60.14 emu/g and coercivity (H_c) between 4274 and 4540 Oe, at 10 K, magnetization data were detected that are much higher with respect to RT values: $M_r = 45.96$–51.06 emu/g, $M_s = 94.42$–95.99 emu/g. The magnetic results indicate that the samples are magnetically hard materials at both considered temperatures. The squareness ratio (SQR) is found to be around 0.50, implying single-domain NPs with uniaxial anisotropy for pristine and substituted samples. With exception, the x = 0.0 sample indicated the formation of multi-domain structure with uniaxial anisotropy at 10 K. Field cooling (FC) susceptibility measurements were applied in temperature range of 5–350 K for pristine sample and samples that contained some Nb^{3+} ions. The analyses of *dc* susceptibility data also proved that Nb^{3+} ion substitution increases the magnetization and, additionally, allows for an easier alignment of the magnetic domains. The obtained magnetic results were investigated deeply with relation to structural and microstructural properties. The observed remanent magnetization (M_r) and coercivity (H_c) render the products are useful for permanent magnets and high-density recording media.

1 Introduction

There are six types of hexaferrites (M, U, W, X, Y, and Z) that differ in their stacking sequences of the three basic blocks (S, R, and T) in their crystal lattices. Among them, M-type hexaferrites are the most important and utilized in several application such as permanent magnetic materials, magneto optical, microwave devices, magnetic recording media and telecommunications devices due to their higher saturation, higher coercivity, room temperature multiferroic properties, better dielectric properties and good chemical stability [1–4]. There are three different types of M-type hexaferrites which are $BaFe_{12}O_{19}$, $SrFe_{12}O_{19}$ and $PbFe_{12}O_{19}$.

The magnetic and electrical properties of M-type hexaferrites can be modified by rare earth metal substitutions like La, Nd, Sm, Ce, Ho, Co, Cu and Cr etc. [5–8]. Previous studies showed an enhancement in magnetic properties of substituted M-type hexaferrites [9–13], with respect to both magneto-crystalline anisotropy and coercive field. Innumerable of researchers have been studied substituted

✉ M. A. Almessiere
malmessiere@iau.edu.sa

✉ Y. Slimani
yaslimani@iau.edu.sa; slimaniyassine18@gmail.com

[1] Department of Nano-Medicine Research, Institute for Research & Medical Consultations (IRMC), Imam Abdulrahman Bin Faisal University, P.O. Box 1982, Dammam 31441, Saudi Arabia

[2] Department of Physics, College of Science, Imam Abdulrahman Bin Faisal University, P.O. Box 1982, Dammam 31441, Saudi Arabia

[3] Department of Biophysics, Institute for Research & Medical Consultations (IRMC), Imam Abdulrahman Bin Faisal University, P.O. Box 1982, Dammam 31441, Saudi Arabia

[4] Institute of Inorganic Chemistry, RWTH Aachen University, 52074 Aachen, Germany

M-type hexagonal. Almessiere et al. [14] are investigated the effect of Nb substitution on morphological, structural and magnetic properties of $BaFe_{12}O_{19}$ hexaferrites. It was observed that the M_s, M_r, n_B and K_{eff} decreased for lower Nb content and then improved on further increasing the Nb concentration. However, H_c was reduced for lower Nb content and was comparable to that of pristine sample for higher contents. Moreover, Yang et al. are reported the Nd and NbZn co-substituted of Sr hexaferrites [15]. They found that the saturation magnetization and magneton number are decreased with increasing Nd and NbZn content. The M_r/M_s ratio, coercivity and magnetic anisotropy field increased with increasing Nd and NbZn content. Sapoletova et al. [16] are discussed the Sb, V and Nb substituted Sr-Zn hexaferrites. The magnetization resualts are increased and decreases with other ratios. The coercive field of the highest saturation magnetization is found to be higher than 3 kOe which lead to be a good candidate for permanent magnet application.

The Fe/Sr molar ratio in the strontium hexaferrites needs to be properly determined in order to obtain single-phase hexagonal ferrite. In order to prepare hexaferrite particles, several synthesis techniques have been developed such as ball milling and mechanical alloying, micro-emulsion co-precipitation, solid-state, sol–gel routes [14–20]. Among these synthesis procedures, the sol–gel method is useful to produce single-domain sized fine powder samples. Thus, in the present study, the low-cost and facile sol–gel auto combustion technique was applied. The magnetic and structural properties of the hexaferrites can be modified for some above-mentioned applications and are mainly dependent on the chemical composition and the way of synthesis [21].

In this study, the effects of doping of Nb^{3+} ions in strontium hexaferrite have been studied by means of structural, morphological and magnetic characterization. An attempt has been made here to evaluate the effect of small addition of the rare earth element Niobium (Nb) on the structural and magnetic properties of Sr hexaferrites.

2 Experimental

2.1 Chemicals and instrumentations

The materials used to synthesize the products, iron(III) nitrate hexahydrate ($Fe(NO_3)_3{\cdot}6H_2O$), barium nitrate ($Ba(NO_3)_2$), niobium chloride ($NbCl_3$) and ammonia (25% v/v, NH_3), all were of analytical grade and obtained from Merck with 99.9% purity.

Phase identification was performed by Rigaku Benchtop Miniflex powder X-ray diffraction (XRD) analyzer with Cu Kα. The microstructure was observed using a field emission scanning electron microscope (FE-SEM) (FEI Titan S/TEM) coupled with energy-dispersive X-ray spectroscopy (EDX). Fourier transform infrared spectra[1] (FTIR; Bruker alpha-II FTIR spectrophotometer attached with a diamond ATR from USA) were recorded using a spectrometer over a range of 2000–400 cm^{-1}. Magnetizations at RT and 10 K and dc susceptibility data for $SrNb_xFe_{12-x}O_{19}$ hexaferrites were obtained using a Quantum Design MPMS-5XL SQUID magnetometer. The polycrystalline samples were compacted and immobilized into cylindrical PTFE capsules. The data were acquired as hysteresis loops (− 5.0 to 5.0 T at 10.0 K and 300 K), and FC measurements (2.0–350 K at 0.05 T). All data were corrected for diamagnetic contributions from the sample holder and the compounds.

2.2 Synthesis

For typical citrate sol–gel auto synthesis, the stoichiometric amount of each metal salt was weighted and dissolved in deionized water under stirring for 40 min. After that citric acid was added to the solution, which was kept stirring at 70 °C until the reaction solution became clear and the pH of the solution was adjusted to seven using aqueous NH_3 solution under stirring. Then the solution was firstly heated to 150 °C, followed by an increase in temperature to 310 °C to allow for complete water evaporation, resulting in a viscous solution. This will turn into an igniting mass that emit lots of gas and will continue to burn and as a result a powder precursor will be obtained. Afterward, this powder was our product.

3 Results and discussion

3.1 XRD analysis

Powder X-ray diffraction patterns of $SrNb_xFe_{12-x}O_{19}$ NHFs are presented in Fig. 1 which the formation of single M-type hexaferrite phase without any additional impurity or secondary phase peaks according to JCPDS file number 79–1411, meaning that the Nb ions are fully incorporated into the Sr hexaferrite lattice. The structure parameters are estimated via the TOPAS refinement program package (Table 1). Although the lattice parameter '*a*' remains constant, the `*c*` parameter increases with increasing Nb ratios, in line with the larger ionic radius of Nb^{3+} (0.72 Å) in comparison to Fe^{3+} (0.64 Å). The *c*/*a* ratio of 3.90 to 3.91 proved also the formation of M-type hexagonal structure [22]. The crystallites size D_{XRD} was calculated by Scherer equation of (114) peak, which is expressed as:

$$D_{XRD} = \frac{0.94\lambda}{\beta \cos\theta}$$

where λ is the X-ray wavelength CuKα radiation (1.5406 Å), β is the line broadening at half the maximum intensity (FWHM), after subtracting the instrumental line broadening, in radians. This quantity is also sometimes denoted as

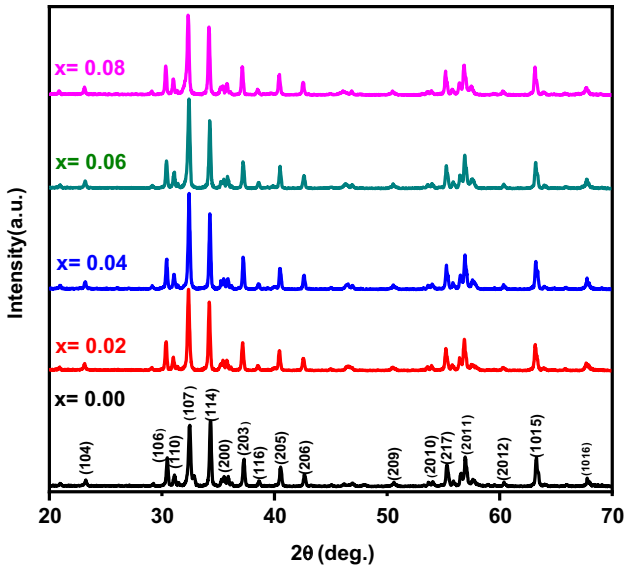

Fig. 1 XRD patterns for $SrNb_xFe_{12-x}O_{19}$ ($0.00 \le x \le 0.08$) hexaferrites

$\Delta(2\theta)$ and θ is the Bragg angle. The crystallites size (D_{XRD}) and the average lattice strain (ε) of the different products were also estimated via the Williamson-Hall equations [23]:

$$\beta = \beta_{strain} + \beta_{size} = 4\varepsilon \tan\theta + \frac{K\lambda}{D_{XRD}\cos\theta}$$

where β is the FWHM of XRD peaks, β_{strain} is the strain broadening that is supposed to be uniform in all crystallographic directions, β_{size} is the particle size broadening, λ is wavelength of CuKα radiation (1.5406 Å), K = 0.94 is a dimensionless shape factor close to unity, and θ is Bragg angle. By multiplying this equation by cos θ, it gives:

$$\beta\cos\theta = 4\varepsilon\sin\theta + \frac{K\lambda}{D_{XRD}}$$

Therefore, by plotting the graph of $\beta\cos\theta$ versus $4\sin\theta$ (Fig. 2), the strain ε of the product is deduced from the slope of linear fitting data (gradient) whereas the D_{XRD} is determined from the Y-intercept ($\frac{K\lambda}{D_{XRD}}$). The estimated values of D_{XRD} and ε deduced by using both Scherrer and Williamson-Hall equations are listed in Table 1. It is clear that the evolution of crystallites size as calculated using both methods showed practically the same trend. However, the D_{XRD} values as calculated using technique are higher than that obtained using Scherrer equation. This mostly due to the fact that only one peak broadening was used for calculation for the Scherrer equation whereas the Williamson–Hall technique takes into consideration of several peaks in order to calculate the crystallize size, which make it more accurate method than Scherrer's method. The D_{XRD} values deduced by using both Scherrer and Williamson-Hall equations are nearly comparable for various concentration and are slightly higher for x = 0.04 and 0.06 samples than to the other concentrations. The determined crystallites size D_{XRD} were found to be good enough making these materials to be used in the high-density recording media (a suitable signal-to-noise ratio). In addition, the value of ε is slightly increased with increasing the Nb^{3+} content.

3.2 FT-IR analysis

FT-IR spectra of $SrNb_xFe_{12-x}O_{19}$ NHFs are depicted in Fig. 3. All compositions exhibited identical spectra and showed a strong vibrations band at 422, 539 and 591 cm^{-1}. These vibration's bands are corresponding to the metal–oxygen bond in tetrahedral and octahedral sites of the Sr-type hexagonal structure [24]. The FTIR spectrum approved the formation of M-type hexaferrite. The vibrational bands of tetrahedral sites are shorter than the octahedral sites due to longer bond length of tetrahedral sites [25]. At x = 0.04 and 0.08, there is a vibration band around 1046 cm^{-1} due to C–C group.

3.3 Morphological analysis

The surface analysis of $SrNb_xFe_{12-x}O_{19}$ hexaferrites is executed via FE-SEM as seen in Fig. 4. All samples presented aggregated particles of hexagonal plate-like structures. It is obvious that the particles size of all compositions is less than 50 nm. EDX spectra and elemental mapping of $SrNb_xFe_{12-x}O_{19}$ ($x = 0.02$ and 0.06) hexaferrites are presented in Fig. 5, detailing the traces of elements that indicated the stoichiometric ratios Sr hexaferrites. Table 2

Table 1 Structural parameters and deduced crystallites size of $SrNb_xFe_{12-x}O_{19}$ ($0.00 \le x \le 0.08$) hexaferrites

x content	*a* = *b* (Å)	*c* (Å)	*c*/*a*	*V* (Å^3)	Scherrer method	Williamson–Hall method	
					D_{XRD} (nm)	D_{XRD} (nm)	Strain $\varepsilon \times 10^{-4}$
0.00	5.882	22.9780	3.90	688.0110	36	57.02	7.303
0.02	5.886	23.0230	3.91	688.2945	36.6	58.7	8.253
0.04	5.880	23.0236	3.91	689.8543	40.8	68.2	8.576
0.06	5.882	23.0292	3.91	690.5587	39.3	67.8	8.977
0.08	5.882	23.0327	3.91	690.6826	37.3	61.0	9.073

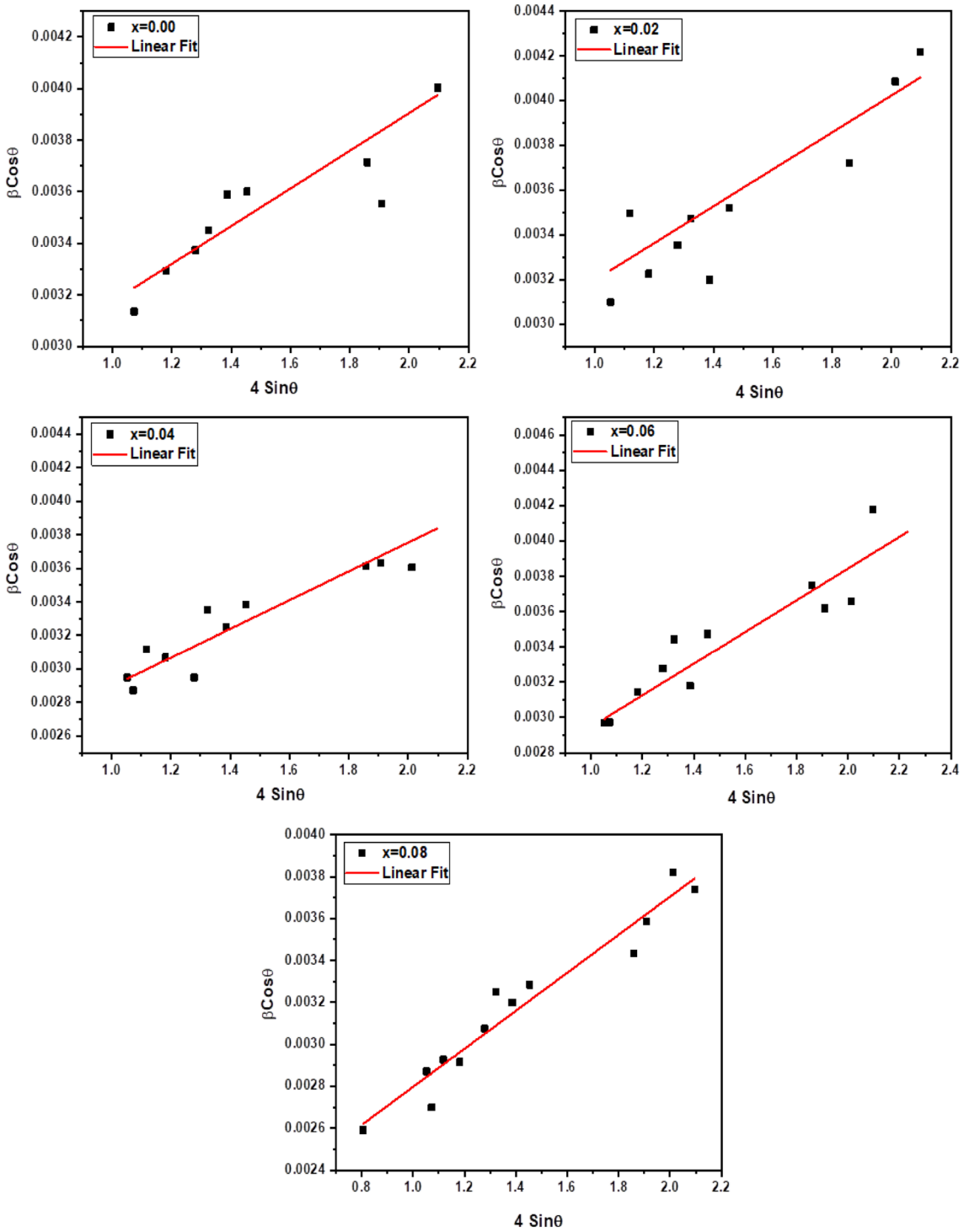

Fig. 2 Williamson-Hall graph for $SrNb_xFe_{12-x}O_{19}$ ($0.00 \leq x \leq 0.08$) hexaferrites

summarizes the theoretical ratio from the molecular weight of element in the molecule and those determined from EDX for all concentrations. The results confirmed the formation of the desired compositions.

3.4 Magnetic properties

Figure 6 presents the specific magnetization hysteresis loops recorded from VSM measurements of $SrNb_xFe_{12-x}O_{19}$ NPs

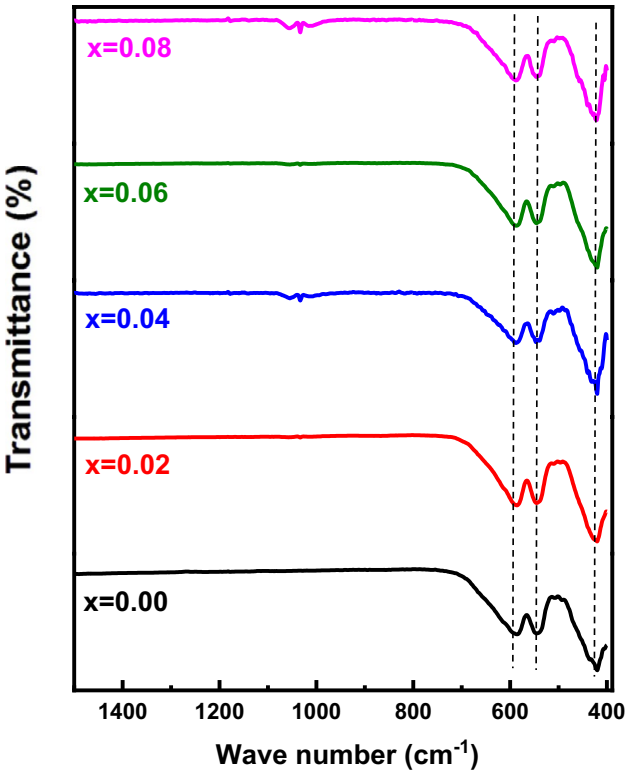

Fig. 3 FT-IR spectra of $SrNb_xFe_{12-x}O_{19}$ ($0.00 \le x \le 0.08$) hexaferrites

as fraction of Nb^{3+} content at room temperature. The hysteresis data were collected by applying an external magnetic field up to ± 10 kOe. The various RT magnetic data derived as fraction of Nb content are given in Table 3. The detailed analyses revealed that the substitution of Fe ions by Nb ions alters in a slight way the magnetization behaviors of the hysteresis loops. The magnitude of magnetizations for applied field of 10 kOe are between 51.70 and 54.41 emu/g. Saturation magnetizations (M_s) were extracted from the linear fits of M versus $1/H^2$ data according to Stoner-Wohlfarth (S-W) theory [26–28]. A typical example of the M against $1/H^2$ plot of x = 0.00 hexaferrite is illustrated in the Fig. 7. The value of M_s is found in the 57.10–60.14 emu/g range. The remanent magnetization (M_r) is ranging between 31.41 and 33.28 emu/g. Coercive fields (H_c) are in a range of 4274–4540 Oe. Accordingly, it can be claimed that the different synthesized samples display ferrimagnetic (FM) behavior at RT. One should note that the M(H) hysteresis loops performed at RT (Fig. 6) clearly indicate the occurrence of a kink around H = 0 kOe in different samples. This observation indicates that some non-magnetic or weak magnetic phases exist in the produced samples. The secondary phases are not noticed by using XRD technique, which is mostly due to the detection limit of the XRD instrument.

The magnetization data were also collected for all $SrNb_xFe_{12-x}O_{19}$ samples at 10 K using SQUID magnetometer by applying field up to ± 20 kOe and are presented in Fig. 8. The entire 10 K magnetic data specified as fraction of Nb^{3+} content are given in Table 4. The pristine $SrFe_{12}O_{19}$ has corresponding magnetization M(H = 10 kOe) = 75.82 emu/g, M_r = 45.96 emu/g, and M_s = 94.42 emu/g. The $SrNb_{0.06}Fe_{11.94}O_{19}$ sample has the maximum magnetization data as $M(H = 10$ kOe) = 80.07 emu/g, M_r = 51.06 emu/g, and M_s = 95.99 emu/g. The coercive field is ranging between 2730 and 3235 Oe for various NPs. In the literature, the M_s magnitudes in an interval between 74.3 and 92.6 emu/g and approximate 6635 Oe of H_c are reported at RT for single crystalline $SrFe_{12}O_{19}$, however the polycrystalline structured samples rarely display values close to these reported maxima [29–32]. In view of the obtained results, it can be claimed that the different produced NPs display also a FM behavior at 10 K. At 10 K, the saturation and remanent magnetizations values are higher than those at RT. The increments in the M_s and M_r values are associated to the reduced thermal changes of surface magnetic moments [33, 34]. In other words, more quantitative ordering of spins in high magnetic fields and at low temperatures contributes to the magnetic moments of the $SrNb_xFe_{12-x}O_{19}$ NPs. However, coercivities are almost equal to half of the reported uppermost RT values. For the same level of Nb^{3+} concentration, the H_c values reduce with decreasing temperature from RT to 10 K. This reduction is correlated with a change in the M_s values. In the case of increment in M_s due to the drop in the temperature, H_c decreases as well [33, 34]. In the current study, the M_s magnitude shows an increase with decreasing temperature from RT to 10 K. Thus, the reduction in H_c may attributable to the increase in M_s as temperature decreases. The observed magnetic parameters render the products useful for magnetic recording media applications. In fact, Numerous studies have revealed that products exhibiting high H_c values are advantageous for magnetic recording applications [35, 36]. They revealed that a longitudinal magnetic recording medium, which is a general type of magnetic recording medium used in industries, requires high enough coercivity (600 Oe). If coercivity is too high (above 1200 Oe), the material can be used for the perpendicular recording media, which is a developing new technology in the magnetic recording media [35, 36]. In the present investigation, the coercivity H_c is in the range of 4274–4540 at RT for various Nb^{3+}-substituted Sr-hexaferrites, which suggests that the prepared products could be applicable in the perpendicular magnetic recording media.

The variation of magnetization data (M_r, M (10 kOe), M_s) as function of Nb^{3+} ion content at 300 K and at 10 K are displayed in Fig. 9a and b, respectively. The minimum M_s values correspond to pristine product (x = 0.00) with magnitudes of about M(10 kOe) = 51.70, M_s = 57.10 and M_r = 31.41 emu/g at RT and M(10 kOe) = 75.82, M_s = 94.42 and M_r = 45.96 emu/g at 10 K. It is clear that

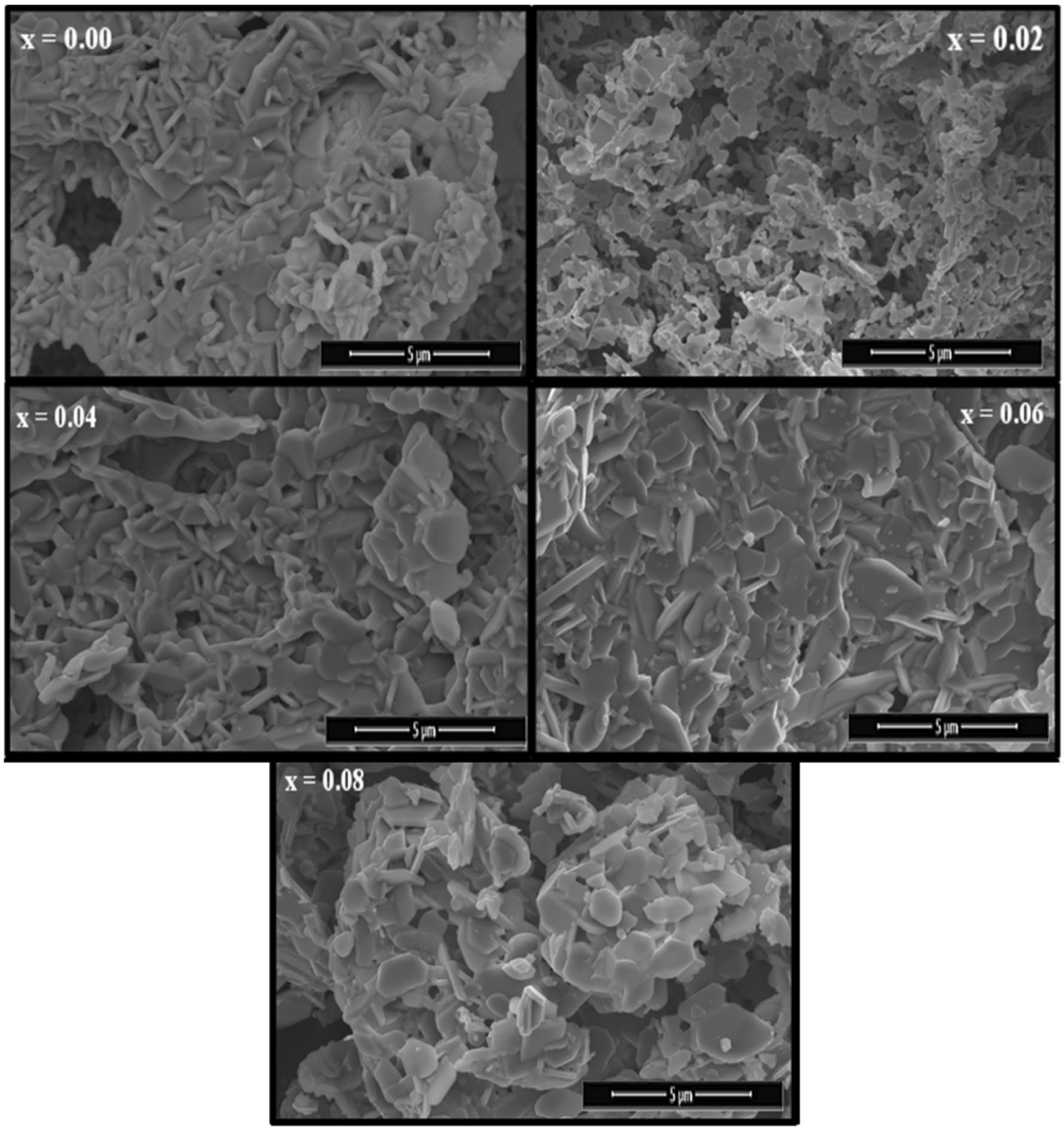

Fig. 4 FE-SEM images of $SrNb_xFe_{12-x}O_{19}$ ($0.00 \leq x \leq 0.08$) hexaferrites

the magnetization data increase with Nb^{3+} substitution at both RT and 10 K. All three magnetization parameters reach maximum values at 300 K for $SrNb_{0.08}Fe_{11.92}O_{19}$ (i.e. $x = 0.08$). However, the magnetic data reach maximum values for $x = 0.06$ at 10 K. The M_s values obtained in this work are important compared to those reported in previous studies of substituted Sr hexaferrites, such as in rare-earth ions substituted $SrFe_{12}O_{19}$ [37, 38] and in Gd-Sn substituted Sr-hexaferrite [39]. The evolutions in M_r values with respect to the Nb concentrations essentially show a similar variation tendency of M_s. Preceding investigations noted that the evolution in the M_r values depends first and foremost on the evolution in M_s values and on the net alignment of grain magnetization caused by the super-exchange interactions among NPs [33, 34].

Usually, numerous factors can affect the magnetic properties of hexaferrites such as the variation in the crystallites size, variations in the magnetic moments (n_B), variations in the nature and concentration of different sites, and preferred site occupancy of different ions, etc. [33, 34]. The disordered cation distributions, formation of local strains, and the super-exchange interactions among various ions could affect also the magnetic properties [40, 41]. The magnetic moment of hexagonal ferrites is derived from the Fe^{3+} ions. The magnetization of the ferrites is mainly ruled by the distribution of Fe ions in the crystal network sites and thus

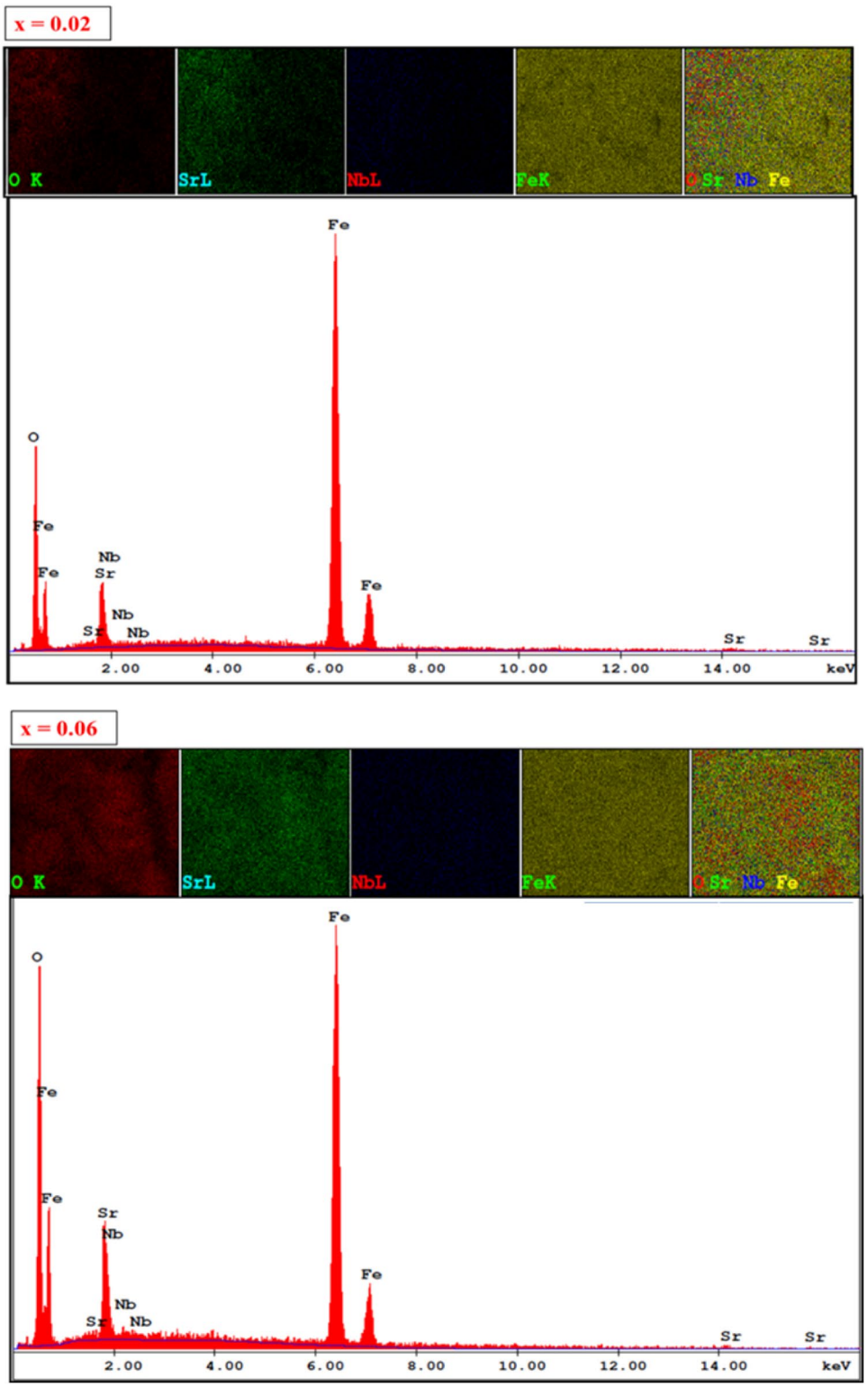

Fig. 5 EDX spectra and elemental mapping of $SrNb_xFe_{12-x}O_{19}$ ($x=0.02$ and 0.06) hexaferrites

changes with the factors that affect the strength of different exchange interactions. It is well known that the Sr^{2+}-O-Sr^{2+} and Sr^{2+}-O-Fe^{3+} interactions are unimportant, however the Fe^{3+}-O-Fe^{3+} exchange interactions are the dominant. Therefore, the increase in the values of M_s and M_r with Nb substitution is attributed to the enhanced exchange of interactions in Fe sites. Also, the site preference of different ions is dependent to the ionic radii of host and substituted ions. Generally, five distinct sub-lattices exist in M-type Sr-hexaferrites: three octahedral (12 k, $4f_2$ and 2a), one

Table 2 Quantitative analyses of various $SrNb_xFe_{12-x}O_{19}$ ($0.00 \le x \le 0.08$) hexaferrites determined from EDX analyses

x content	Theoretical compositions				Weight % determined by EDX			
	Sr	Nb	Fe	O	Sr	Nb	Fe	O
0.00	8.25	0.00	63.12	28.63	8.35	0.00	63.65	28.00
0.02	8.25	0.17	62.97	28.61	8.44	0.22	63.45	27.89
0.04	8.24	0.35	62.82	28.59	8.49	0.45	63.06	28.00
0.06	8.24	0.52	62.67	28.57	8.54	0.71	62.85	27.70
0.08	8.23	0.70	62.52	28.55	8.68	1.02	62.25	28.05

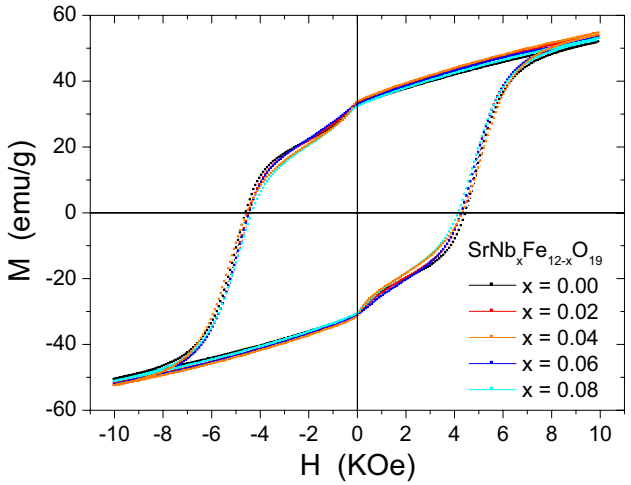

Fig. 6 VSM hysteresis loops of $SrNb_xFe_{12-x}O_{19}$ ($0.00 \le x \le 0.08$) hexaferrites performed at 300 K

trigonal-bi-pyramidal (2b) and one tetrahedral ($4f_1$) sites. The magnetic moment is derived from the Fe^{3+} ions, which reside in the five different sub-lattices. Fe^{3+} ions in $4f_1$ and $4f_2$ sites have spins-down, while those in 2a, 2b and 12 k sites have spins-up. Thus, the magnetization is the result of the difference between the spins-up and spins-down of magnetic moments. The magnetization of the hexagonal ferrites depends on the factors that affect the Fe^{3+}-O-Fe^{3+} exchange interactions strength. If the substitution was done in the spin-up sites, the magnetization decreases [33, 34]. However, if the substitution was done in the spin-down sites, the magnetization increases [33, 34]. The ionic radii of different ions are equal to $r_{Nb^{3+}} = 0.72$Å, $r_{Fe^{3+}} = 0.64$Å, $r_{Sr^{2+}} = 1.26$Å, respectively. The Nb^{3+} ions have ion radius closer to Fe^{3+} than to Sr^{2+}, hence one could anticipate that the Nb^{3+} ions will prefer to reside in the Fe^{3+} sites. Furthermore, it can be assumed that the Nb^{3+} ions substitute the spin-down iron sites.

On other hand, we note that the Nb^{3+} ion radius (0.72 Å) slightly exceeds that of Fe^{3+} (0.64 Å). The non-equivalent ionic radius and magnetic moments of the host and substituted ions could generate local strain that causes a variation of electronic states and disorder in the hexaferrite system [33, 34]. In addition, substituting Fe^{3+} ions by Nb^{3+} results in a reducing the distance separating the magnetic ions and therefore increasing the super-exchange interactions strength. Furthermore, the variations in the magnetic moments could explain the behavior of the magnetization magnitudes. The experimental values of the magneton numbers, n_B, in units of μ_B by formula unit are deduced as follow [41]:

$$n_B = \frac{Molecular\ weight \times M_s}{5585}$$

The estimated n_B values for $SrNb_xFe_{12-x}O_{19}$ NPs at different temperatures are present in Tables 3 and 4, respectively. Generally, the strengthening of the super-exchange interactions among the various sites lead to an increase in n_B values. In the present study, the evaluated n_B increases slightly from 10.85 to 11.46 μ_B at RT and from 17.95 to 18.28 at 10 K. It was found that the product with the highest M_s value exhibits the highest n_B value. This is a consequence of the intensification of super-exchange interactions. It is noticed the disappearance of the kink at 10 K (Fig. 8), which could be attributed the reduced thermal fluctuations at low temperature. Taking into account the magnetic structure of M-type strontium

Table 3 The deduced magnetic parameters of $SrNb_xFe_{12-x}O_{19}$ ($0.00 \le x \le 0.08$)) hexaferrites at 300 K

x	MW (g/mol)	M ($H = 10$ kOe) (emu/g)	M_s (emu/g)	M_r (emu/g)	SQR	H_c (Oe)	n_B^* (μ_B)
0.00	1061.76	51.70	57.10	31.41	0.550	4540	10.85
0.02	1062.50	53.45	58.47	32.74	0.562	4410	11.12
0.04	1063.24	52.88	58.36	32.46	0.556	4385	11.11
0.06	1063.98	52.73	58.46	31.87	0.545	4274	11.13
0.08	1064.72	54.41	60.14	35.62	0.553	4487	11.46

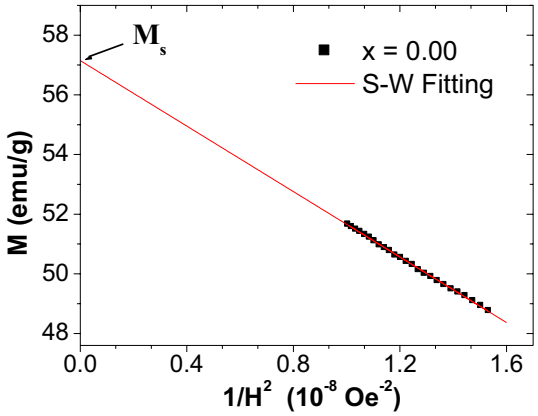

Fig. 7 Plot of M versus $1/H^2$ of $SrFe_{12}O_4$ (x = 0.00) hexaferrite. The solid line corresponds to the S-W fitting

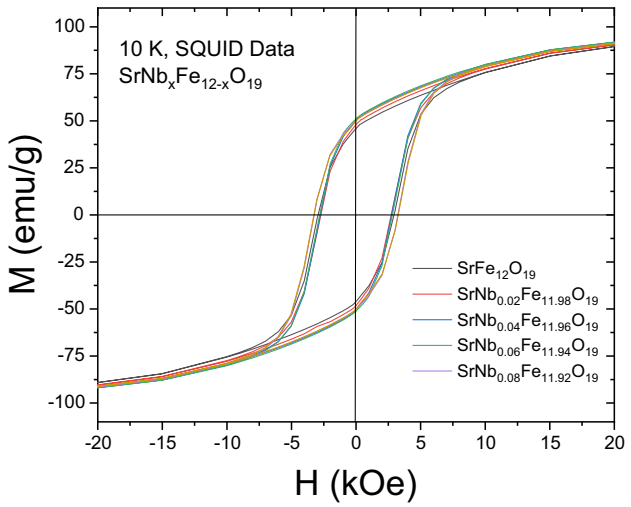

Fig. 8 Magnetic hysteresis loops of $SrNb_xFe_{12-x}O_{19}$ ($0.00 \le x \le 0.08$) hexaferrites at 10 K

hexaferrites consisting of iron with spins-down on $4f_1$ and $4f_2$ sites and spins-up on 12 k, 2a and 2b sites, the moment per formula unit will be about 20 μ_B for pristine Sr-hexaferrites (x = 0.0) [42, 43]. Nevertheless, the obtained experimental n_B values are in the range 10.85–11.46 μ_B and 17.95–18.28 at both considered temperatures which is lower than 20 μ_B, indicating that evident non-magnetic or weak magnetic content exist in the samples.

The squareness ratios ($SQR = M_r/M_s$) were determined for all $SrNb_xFe_{12-x}O_{19}$ NPs at 300 and 10 K (see Tables 3 and 4). The SQRs take proximate values of 0.500 and 0.830 for uniaxial and cubic anisotropy, respectively according to Stoner-Wohlfart theory [44]. Additionally, when the SQR is greater than 0.5, the NPs are considered to be in a single magnetic domain [45]. However, when SQR is inferior than 0.5, the NPs are generally considered to be in multi magnetic domains [45]. All $SrNb_xFe_{12-x}O_{19}$ NPs display SQRs > 0.5 at both RT and 10 K, specifying the single-domain structure characteristics with uniaxial anisotropy. With exception, the x = 0.0 NPs showed SQR value < 0.5 at 10 K, which indicates the formation of multi-domain structure with uniaxial anisotropy at 10 K.

At RT, the H_c value is maximum for pristine sample and decreases with Nb^{3+} substitution. Among substituted samples, the x = 0.08 has the maximum H_c at RT. At low temperature, the coercive field H_c is determined as 2945 Oe for pristine sample, however a ~ 200 Oe decrease in coercivity of samples with $x = 0.02$–0.06 and a ~ 200 Oe gain in coercivity of samples with $x = 0.08$ were observed. Frequently, the coercivity is dependent to numerous parameters such as the morphology, shape anisotropy, magnetocrystalline anisotropy, size distributions, grains size and exchange coupling among the canted spins on the surface and the collinear spins in the core, etc. [46, 47].

We performed field cooled (FC) *dc* susceptibility measurements on three samples ($x = 0.00$, 0.02 and 0.04), see Fig. 10. Therefore, we applied a *dc* magnetic field of 500 Oe at 350 K and measured the susceptibility with decreasing temperatures down to 2 K. This procedure allows for the temperature dependent characterization at a constant field complementary to hysteresis measurements for which the temperature is constant and the field varies. For temperatures below 350 K, the χ_g versus T curves show similar shape characteristics. χ_g linearly increases from 350 K to ca. 80 K, and reaches a plateau for $T < 40$ K. Without any Nb^{3+} ion content ($x = 0$), the values of χ_g (0.008 to 0.011 emu/g) are smaller compared to the values of the compounds including Nb^{3+} ions. For $x = 0.02$ and 0.04 substitution levels, χ_g ranges from 0.038 to 0.060 emu/g and 0.045 to 0.073 emu/g,

Table 4 The deduced magnetic parameters of $SrNb_xFe_{12-x}O_{19}$ ($0.00 \le x \le 0.08$) hexaferrites at 10 K

x	MW (g/mol)	*M* (*H* = 10 kOe) (emu/g)	M_s (emu/g)	M_r (emu/g)	SQR	H_c (Oe)	n_B^* (μ_B)
0.00	1061.76	75.82	94.42	45.96	0.486	2945	17.95
0.02	1062.50	77.89	94.92	48.01	0.505	2730	18.06
0.04	1063.24	79.44	95.36	50.25	0.527	2760	18.15
0.06	1063.98	80.07	95.99	51.06	0.532	2820	18.28
0.08	1064.72	79.32	95.52	50.14	0.525	3235	19.21

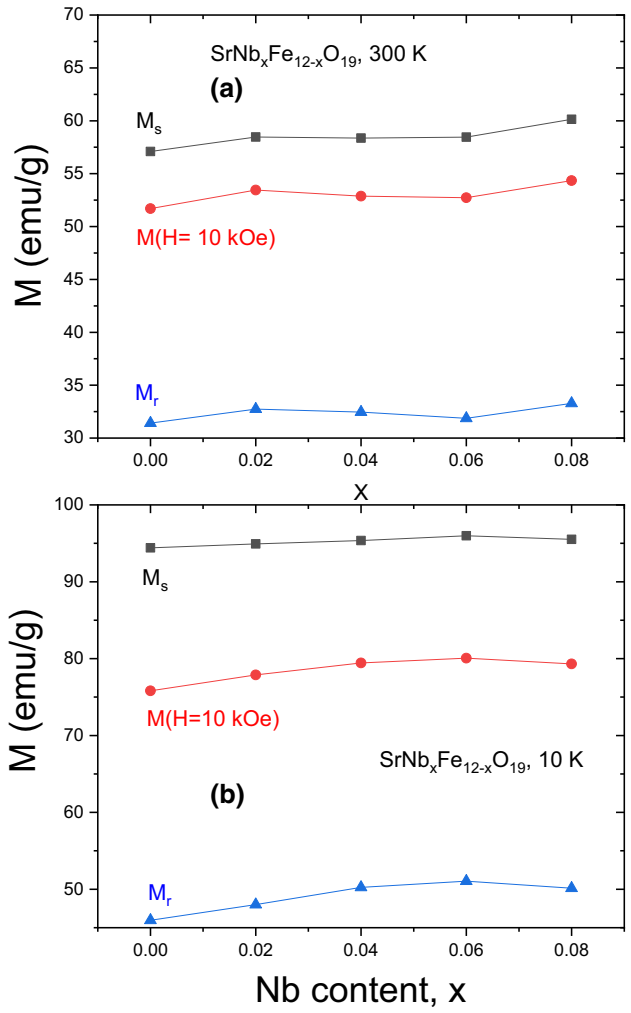

Fig. 9 Magnetization data of $SrNb_xFe_{12-x}O_{19}$ ($0.00 \le x \le 0.08$) hexaferrites as function of Nb^{3+} content **a** at 300 K and **b** at 10 K

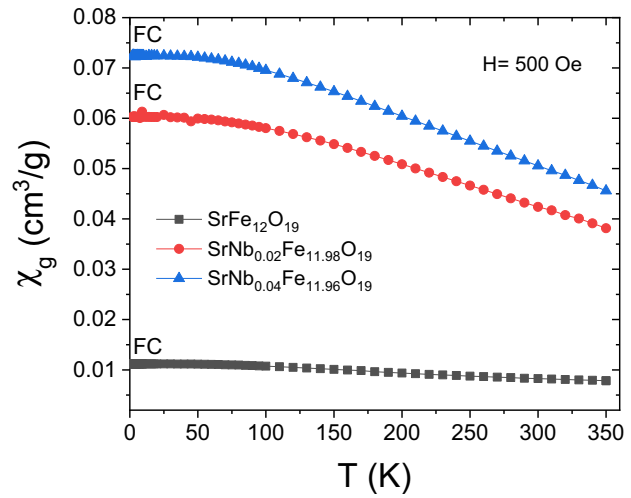

Fig. 10 Field cooling measurements: temperature dependence of χ_g for selected $SrNb_xFe_{12-x}O_{19}$ samples at 0.05 T

respectively. Thus, the higher Nb^{3+} ion content, the larger the χ_g value of the plateaus. This is to some degree also reflected in the values of the remanence magnetization, although the values at 2.0 K are distinctly below the remanence due to measuring in the initial magnetization region of a hysteresis loop. The VSM measurements, on the other hand, show the results for measurements where the saturation has been reached, i.e. the real remanence magnetization and we do not show the initial magnetization curve there. That is why the values at 2.0 K of χ_g are much smaller than the corresponding value derived from the remanence. Hence, *dc* susceptibility measurements also reveal that the Nb^{3+} ion content slightly increases the magnetization and, additionally, allows for an easier alignment of the magnetic domains. On the other side, the M_{FC} curves increase continuously with reducing the temperature and at a certain temperature they become constant. Numerous studies reported that the M_{FC} curves increases continuously in SPM nano-sized particles, however they show a slowest increase or a flat nature in super-spin glass (SSG) systems because of the strong interactions between nanoparticles [48, 49]. In view of that, the observed flat nature at lower temperatures in the curves of M_{FC} reveals the existence of a SSG-like state. Similar behaviors have been reported in other ferrites [48–50].

4 Conclusion

This study describes in detail the structure, microstructure and magnetic characteristics of $SrNb_xFe_{12-x}O_{19}$ ($0.00 \le x \le 0.08$) NHFs. The XRD, FTIR, and SEM along with EDX analyses confirmed the formation of the desired compositions. All substitution levels resulted in increasing the lattice parameter *c*. The crystallites sizes are ranging between 35.3 and 40.8 nm. *M*(*H*) hysteresis curves of all $SrNb_xFe_{12-x}O_{19}$ ($0.00 \le x \le 0.08$) NHFs were recorded at 300 and at 10 K and analyzed with the field cooling *dc* susceptibility data of some samples ($x = 0.00, 0.02, 0.04$). All specified magnetic data reveal the hard ferrimagnetic nature of various prepared samples. Nb^{3+} ion substitution slightly increases marginally the magnetization magnitude with respect to pristine sample. However, we observe slight changes in coercivity values depending on the ion composition. The deduced M(10 kOe), M_s, and M_r values are maximum for x = 0.08 and 0.06 samples at RT and 10 K, respectively. This effect is due to the reinforcement of superexchange interactions, the creation of local strains, the preferred site occupancy and the increase in the magnetic moments (n_B) in this sample. The evaluated SQRs at around 0.5 point to single-domain nanoparticles having uniaxial magnetic anisotropy according to the S-W model, except the x = 0.0 sample that indicated the formation of multi-domain structure with uniaxial anisotropy at 10 K. The observed M_r

and H_c render the products useful for permanent magnets and high-density recording media applications.

Acknowledgements The authors highly acknowledged the financial supports of the Institute for Research and Medical Consultations of Imam Abdulrahman Bin Faisal University—Saudi Arabia (Projects Nos. 2018-IRMC-S-2, 2018-IRMC-S-1 and 2017-IRMC-S-3).

References

1. L. Lechevallier, J.M. Le Breton, A. Morel, J. Teillet, Structural and magnetic properties of Sr1-xSmxFe12O19 hexagonal ferrites synthesised by a ceramic process. J. Alloys Compd. **359**, 310–314 (2003)
2. H. Mocuta, L. Lechevallier, J.M. Le Breton, J.F. Wang, I.R. Harris, Structural and magnetic properties of hydrothermally synthesized $Sr_{1-x}Nd_xFe_{12}O_{19}$ hexagonal ferrites. J. Alloys Compd. **364**, 48–52 (2004)
3. R.C. Pullar, Hexagonal ferrites: a review of the synthesis, properties and applications of hexaferrite ceramics. Prog. Mater Sci. **57**, 1191–1334 (2012)
4. R.C. Pullar, Hexagonal ferrites: a review of the synthesis, properties and applications of hexaferrite ceramics. Prog. Mater Sci. **57**, 1191–1334 (2012)
5. D.A. Vinnik, A.S. Semisalova, L.S. Mashkovtseva, A.K. Yakushechkina, S. Nemrava, S.A. Gudkova, D.A. Zherebtsov, N.S. Perov, L.I. Isaenko, R. Niewa, Structural and magnetic characterization of Zn-substituted barium hexaferrite single crystals. Mater. Chem. Phys. **163**, 416–420 (2015)
6. X.-S. Liu, L. Fetnandez-Garcia, F. Hu, D.-R. Zhu, M. Suarez, J.L. Menendez, Magneto-optical Kerr spectra and magnetic properties of Co-substituted Mtype strontium ferrites. Mater. Chem. Phys. **133**, 961–964 (2012)
7. S. Vadivelan, N.V. Jaya, Investigation of magnetic and structural properties of copper substituted barium ferrite powder particles via co-precipitation. Res. Phys. **6**, 843–850 (2016)
8. S. Katlakunta, S.S. Meena, S. Sirnath, M. Bououdina, R. Sandhya, K. Praveena, Improved magnetic properties of Cr3 doped SrFe12O19 via microwave hydrothermal route. Mater. Res. Bull. **63**, 58–66 (2015)
9. I.A. Auwal, A. Baykal, H. Güngüneş, S.E. Shirsath, Structural investigation and hyperfine interactions of $BaBi_xLa_xFe_{12-2x}O_{19}$ ($0.0 \le x \le 0.5$) hexaferrites. Ceram. Int. **42**, 3380–3387 (2016)
10. R. Topkaya, I. Auwal, A. Baykal, Effect of temperature on magnetic properties of BaYxFe12-xO19 hexaferrites. Ceram. Int. **42**(14), 16296–16302 (2016)
11. Y. Yang, F. Wang, J. Shao, D. Huang, H. He, A.V. Trukhanov, S.V. Trukhanov, Influence of Nd-NbZn co-substitution on structural, spectral and magnetic properties of M-type calcium-strontium hexaferrites Ca0.4Sr0.6-xNdxFe12.0-x(Nb0.5Zn0.5)xO1.9. J. Alloys Compd. **765**, 616–623 (2018)
12. M.A. Almessiere, Y. Slimani, A. Baykal, Impact of Nd-Zn co-substitution on microstructure and magnetic properties of $SrFe_{12}O_{19}$ nanohexaferrite. Ceram. Int. **45**, 963–969 (2019)
13. M.A. Almessiere, Y. Slimani, H. Güngüneş, A. Baykal, S.V. Trukhanov, A.V. Trukhanov, Manganese/yttrium codoped strontium nanohexaferrites: evaluation of magnetic susceptibility and mossbauer spectra. Nanomaterials **9**, 24 (2019)
14. R.B. Jotania, R.B. Khomane, C.C. Chauhan, S.K. Menon, B.D. Kulkarni, Synthesis and magnetic properties of barium–calcium hexaferrite particles prepared by sol–gel and microemulsion techniques. J. Magn. Magn. Mater. **320**, 1095–1101 (2008)
15. Y. Yang, F. Wang, J. Shao, D. Huang, H. He, A.V. Trukhanov, S.V. Trukhanov, Influence of Nd-NbZn co-substitution on structural, spectral and magnetic properties of M-type calcium-strontium hexaferrites Ca0.4Sr0.6-xNdxFe12.0-x(Nb0.5Zn0.5)xO19. J. Alloys Compd. **765**, 616–623 (2018)
16. N. Sapoletova, S. Kushnir, K. Ahn, S.Y. An, M. Choi, J.Y. Kim, C. Choi, S. Wi, M-Zn (M = Sb, V, and Nb) substituted strontium hexaferrites with enhanced saturation magnetization for permanent magnet applications. J. Magn. **21**(3), 315–321 (2016)
17. H. Yanbing, J. Sha, S. Lina, T. Quan, L. Qin, J. Hongxiao, J. Dingfeng, B. Hong, G. Hongliang, X. Wang, Tailored magnetic properties of Sm(Zn) substituted nanocrystalline barium hexaferrites. J. Alloys Compd. **486**, 348–351 (2009)
18. M.J. Iqbal, S. Farooq, Extraordinary role of Ce–Ni elements on the electrical and magnetic properties of Sr–Ba M-type hexaferrites. Mater. Res. Bull. **44**, 2050–2055 (2009)
19. I. Bsoul, S.H. Mahmood, Magnetic and structural properties of BaFe12−xGaxO19 nanoparticles. J. Alloys Compd. **489**, 110–114 (2010)
20. M.A. Almessiere, Y. Slimani, N.A. Tashkandi, A. Baykal, M.F. Saraç, A.V. Trukhanov, İ. Ercan, İ. Belenli, B. Ozçelik, The effect of Nb substitution on magnetic properties of BaFe12O19 nanohexaferrites. Ceram. Int. **45**, 1691–1697 (2019)
21. M.A. Almessiere, Y. Slimani, H.S. El Sayed, A. Baykal, Ca^{2+} and Mg^{2+} incorporated barium hexaferrites: structural and magnetic properties. J. Sol-Gel Sci. Tech. **88**, 628–638 (2018)
22. M.A. Almessiere, Y. Slimani, H.S. El Sayed, A. Baykal, S. Ali, I. Ercan, Investigation of microstructural and magnetic properties of $BaV_xFe_{12-x}O_{19}$ nanohexaferrites. J. Supercond. Nov. Magn. (2018). https://doi.org/10.1007/s10948-018-4856-8
23. Y. Slimani, M.A. Almessiere, E. Hannachi, A. Baykal, A. Manikandan, M. Mumtaz, F.B. Azzouz, Influence of WO_3 nanowires on structural, morphological and flux pinning ability of $YBa_2Cu_3O_y$ superconductor. Ceram. Int. **45**, 2621–2628 (2019)
24. A. Thakur, R.R. Singh, P.B. Barman, Synthesis and characterizations of Nd^{3+} doped $SrFe_{12}O_{19}$ nanoparticles. Mater. Chem. Phys. **141**, 562–569 (2013)
25. S.M. El-Sayed, T.M. Meaz, M.A. Amer, H.A. El Shersaby, Magnetic behavior and dielectric properties of aluminum substituted M-type barium hexaferrite. Phys. B **426**, 137–143 (2013)
26. E.C. Stoner, E.P. Wohlfarth, A mechanism of magnetic hysteresis in heterogeneous alloys. Philos. Trans. R. Soc. A **240**(826), 599–642 (1948)
27. M.A. Almessiere, Y. Slimani, S. Ali, A. Baykal, I. Ercan, H. Sozeri, Nd^{3+} ion-substituted $Co_{1-2x}Ni_xMn_xFe_{2-y}Nd_yO_4$ nanoparticles: structural, morphological, and magnetic investigations. J. Inorg. Organomet. Polym. (2018). https://doi.org/10.1007/s10904-018-1052-z
28. M.A. Almessiere, Y. Slimani, A. Baykal, Structural, morphological and magnetic properties of hard/soft $SrFe_{12-x}V_xO_{19}/(Ni_{0.5}Mn_{0.5}Fe_2O_4)_y$ nanocomposites: effect of vanadium substitution. J. Alloy. Compd. **767**, 966–975 (2018)
29. H. Kojima, E.P. Wohlfarth, *Ferromagnetic materials*, vol. 3 (North-magneto-optical recording Holland, Amsterdam, 1982), p. 305
30. M.M. Hessien, M.M. Rashad, K. El-Barawy, Controlling the composition and magnetic properties of strontium hexaferrite synthesized by co-precipitation method. J. Magn. Magn. Mater. **32**, 336–343 (2008)
31. H. Kojima, E.P. Wohlfarth, *Ferromagnetic Materials*, vol. 3 (North-magneto-optical recording Holland, Amsterdam, 1982), p. 305
32. M.M. Hessien, M.M. Rashad, K. El-Barawy, Controlling the composition and magnetic properties of strontium hexaferrite synthesized by co-precipitation method. J. Magn. Magn. Mater. **32**, 336–343 (2008)

33. Z. Durmus, H. Kavas, A. Durmus, B. Aktaş, Synthesis and microstructural characterization of grapheme/strontium hexaferrite ($SrFe_{12}O_{19}$) nanocomposites. Mater. Chem. Phys. **163**, 439–445 (2015)
34. M.A. Almessiere, Y. Slimani, H.S. El Sayed, A. Baykal, Structural and magnetic properties of Ce-Y substituted strontium nanohexaferrites. Ceram. Int. **44**, 12511–12519 (2018)
35. M.N. Ashiq, M.J. Iqbal, M. Najam-ul-Haq, P.H. Gomez, A.M. Qureshi, Synthesis, magnetic and dielectric properties of Er–Ni doped Sr-hexaferrite nanomaterials for applications in high density recording media and microwave devices. J. Magn. Magn. Mater. **324**, 15–19 (2012)
36. Y. Li, R. Liu, Z. Zhang, C. Xiong, Hydration resistance of AlN powder and the application of AlN powder to corundum spinel castables. Mater. Chem. Phys. **64**, 256 (2000)
37. M.A. Almessiere, Y. Slimani, A. Baykal, Structural and magnetic properties of Ce doped strontium hexaferrite. Ceram. Int. **44**, 9000 (2018)
38. M.A. Almessiere, Y. Slimani, H.S. El Sayed, A. Baykal, I. Ercan, Microstructural and magnetic investigation of vanadium-substituted Sr-nanohexaferrite. J. Magn. Magn. Mater. **471**, 124–132 (2019)
39. M.N. Ashiq, S. Shakoor, M. Najam-ul-Haq, M.F. Warsi, I. Ali, I. Shakird, Structural, electrical, dielectric and magnetic properties of Gd-Sn substituted Sr-hexaferrite synthesized by sol–gel combustion method. J. Magn. Magn. Mater. **374**, 173–178 (2015)
40. M.A. Almessiere, Y. Slimani, H.S. El Sayed, A. Baykal, Morphology and magnetic traits of strontium nanohexaferrites: effects of manganese/yttrium co-substitution. J. Rare Earths (2019). https://doi.org/10.1016/j.jre.2018.09.014
41. M.A. Almessiere, Y. Slimani, A. Baykal, Impact of Nd-Zn co-substitution on microstructure and magnetic properties of $SrFe_{12}O_{19}$ nanohexaferrite. Ceram. Int. **45**, 963–969 (2019)
42. D. Seifert, J. Töpfer, F. Langenhorst, J.-M. Le Breton, H. Chiron, L. Lechevallier, Synthesis and magnetic properties of La-substituted M-type Sr hexaferrites. J. Magn. Magn. Mater. **321**, 4045–4051 (2009)
43. M.N. Ashiq, M.J. Iqbal, I.H. Gul, Effect of Al–Cr doping on the structural, magnetic and dielectric properties of strontium hexaferrite nanomaterials. J. Magn. Magn. Mater. **323**, 259–263 (2011)
44. M.A. Almessiere, A.D. Korkmaz, Y. Slimani, M. Nawaz, S. Ali, A. Baykal, Magneto-optical properties of rare earth metals substituted Co-Zn spinel nanoferrites. Ceram. Int. **45**, 3449–3458 (2019)
45. I. Ali, M.U. Islam, M.S. Awan, M. Ahmad, M.N. Ashiq, S. Naseem, Effect of Tb^{3+} substitution on the structural and magnetic properties of M-type hexaferrites synthesized by sol–gel autocombustion technique. J. Alloy. Compd. **550**, 564–572 (2013)
46. Y. Slimani, H. Güngüneş, M. Nawaz, A. Manikandan, H.S. El Sayed, M.A. Almessiere, H. Sözeri, S.E. Shirsath, I. Ercan, A. Baykal, Magneto-optical and microstructural properties of spinel cubic copper ferrites with Li-Al co-substitution. Ceram. Int. **44**, 14242 (2018)
47. M. Amir, H. Gungunes, Y. Slimani, N. Tashkandi, H.S. El Sayed, F. Aldakheel, M. Sertkol, H. Sozeri, A. Manikandan, I. Ercan, A. Baykal, Mossbauer studies and magnetic properties of cubic $CuFe_2O_4$ nanoparticles. J. Supercond. Novel Magn. **5**, 4 (2018). https://doi.org/10.1007/s10948-018-4733-5
48. D. Peddis, C. Cannas, G. Piccaluga, E. Agostinelli, D. Fiorani, Surface spin freezing effects on enhanced saturation magnetization and magnetic anisotropy in $CoFe_2O_4$ nanoparticles. Nanotechnology **21**, 125705 (2010)
49. X. Chen, S. Bedanta, O. Petracic, W. Kleemann, S. Sahoo, S. Cardoso, P. Freitas, Superparamagnetism versus superspin glass behavior in dilute magnetic nanoparticle systems. Phys. Rev. B **72**, 214436 (2005)
50. M.A. Almessiere, Y. Slimani, H. Güngüneş, H.S. El Sayed, A. Baykal, AC susceptibility and hyperfine interactions of vanadium substituted barium nanohexaferrites. Ceram. Int. **44**, 17749–17758 (2018)